


Research Paper

^{52}Mn Production for PET/MRI Tracking Of Human Stem Cells Expressing Divalent Metal Transporter 1 (DMT1)

Christina M. Lewis^{*1}, Stephen A. Graves^{*1}, Reinier Hernandez¹, Hector F. Valdovinos¹, Todd E. Barnhart¹, Weibo Cai^{1,2,3}, Mary E. Meyerand^{1,2,4}, Robert J. Nickles¹, Masatoshi Suzuki⁵ 

1. Department of Medical Physics, University of Wisconsin - Madison, Madison, WI, USA;
2. Department of Radiology, University of Wisconsin - Madison, Madison, WI, USA;
3. Carbone Cancer Center, University of Wisconsin - Madison, Madison, WI, USA;
4. Department of Biomedical Engineering, University of Wisconsin - Madison, Madison, WI, USA;
5. Department of Comparative Biosciences, University of Wisconsin - Madison, Madison, WI, USA.

* Authors contributed equally to this work.

 Corresponding author: Masatoshi Suzuki, 4124 Veterinary Medicine Building, 2015 Linden Drive, Madison, WI 53706, USA. Tel: (608) 262-4264; Fax: (608) 890-3667; E-mail: msuzuki@svm.vetmed.wisc.edu.

© Ivyspring International Publisher. This is an open-access article distributed under the terms of the Creative Commons License (<http://creativecommons.org/licenses/by-nc-nd/3.0/>). Reproduction is permitted for personal, noncommercial use, provided that the article is in whole, unmodified, and properly cited.

Received: 2014.07.24; Accepted: 2014.10.22; Published: 2015.01.01

Abstract

There is a growing demand for long-term *in vivo* stem cell imaging for assessing cell therapy techniques and guiding therapeutic decisions. This work develops the production of ^{52}Mn and establishes proof of concept for the use of divalent metal transporter 1 (DMT1) as a positron emission tomography (PET) and magnetic resonance imaging (MRI) reporter gene for stem cell tracking in the rat brain. ^{52}Mn was produced via proton irradiation of a natural chromium target. In a comparison of two ^{52}Mn separation methods, solvent-solvent extraction was preferred over ion exchange chromatography because of reduced chromium impurities and higher ^{52}Mn recovery. *In vitro* uptake of Mn-based PET and MRI contrast agents ($^{52}\text{Mn}^{2+}$ and Mn^{2+} , respectively) was enhanced in DMT1 over-expressing human neural progenitor cells (hNPC-DMT1) compared to wild-type control cells (hNPC-WT). After cell transplantation in the rat striatum, increased uptake of Mn-based contrast agents in grafted hNPC-DMT1 was detected in *in vivo* manganese-enhanced MRI (MEMRI) and *ex vivo* PET and autoradiography. These initial studies indicate that this approach holds promise for dual-modality PET/MR tracking of transplanted stem cells in the central nervous system and prompt further investigation into the clinical applicability of this technique.

Key words: Positron emission tomography (PET), manganese-enhanced magnetic resonance imaging (MEMRI), multimodality imaging, manganese-52 (^{52}Mn), cell tracking, reporter gene.

Introduction

The growing field of stem cell therapy is moving toward clinical trials in a variety of applications, particularly for cardiac and neurological diseases [1, 2]. This translation of cell therapies into humans has prompted a need to assess the location, survival, and dynamics of transplanted cells non-invasively and longitudinally.

In recent years, a variety of *in vivo* cell tracking methods have been developed and applied in animals

and humans, including direct labeling with superparamagnetic iron oxide nanoparticles (SPIO) [3, 4] and radiolabelled molecules such as ^{111}In -oxine and ^{18}F -FDG [5, 6]. The direct labeling approach for cell tracking is relatively straightforward, clinically applicable, and well suited for short-term studies to investigate the initial distribution of cells. However, the potential for long-term cell tracking can be compromised by radiolabel decay, label dilution upon cell

division, non-specific contrast if the label leaves the cell, and label persistence upon cell death [7]. Reporter genes present an alternative approach to stem cell tracking that can offer greater depth of functional information regarding cell survival and differentiation [8, 9]. Several reporter genes have been extensively investigated for this purpose, most notably firefly luciferase for bioluminescence imaging (BLI), herpes simplex virus-1 thymidine kinase (HSV-TK) for PET, and ferritin for MRI [8, 10, 11]. These reporters have had varying success, and they each have their own strengths and weaknesses in terms of sensitivity, clinical applicability, soft tissue contrast, resolution, and applicability in the central nervous system [12].

In this work, we investigate the divalent metal transporter 1 as a reporter gene for cell tracking in the central nervous system. The DMT1 protein transports divalent metals such as Cd^{2+} , Fe^{2+} , Co^{2+} , and Mn^{2+} [13]. This protein is ubiquitously expressed and plays important roles in metal transport in the brain and gut, with relatively lower expression levels in the brain [14]. As a reporter gene, DMT1 over-expression enables increased manganese (Mn) incorporation, resulting in selective signal enhancement and detection in MRI [15]. Although several groups of researchers have investigated Mn-based MRI for cellular imaging [15, 16], we hypothesize that ^{52}Mn -based PET could offer increased sensitivity, reduced bulk manganese dose, and provide valuable complementary information when paired with manganese-enhanced MRI (MEMRI).

Radio-manganese (^{51}Mn and ^{52m}Mn) was first used as a myocardial perfusion PET agent by Daube and colleagues in 1985 [17], with successful studies conducted in humans. More recently ^{52}Mn ($t_{1/2} = 5.591$ d, $\beta^+ = 29.6\%$, $E(\beta^+)_{\text{max}} = 0.576$ MeV) has presented itself as a strong candidate for PET applications. The half-life and favorable low maximum positron energy of ^{52}Mn allow for superb imaging resolution, comparable to ^{18}F , several days after systemic injection [18]. Furthermore, ^{52}Mn could be substituted for or supplemented with natural Mn in previously developed MEMRI applications [19, 20]. ^{52}Mn is produced by irradiating chromium targets with 10-20 MeV protons, and separation has previously been achieved by ion exchange chromatography [18]. Alternative methods employ the organic extractant trioctylamine (TOA) and may be more viable for producing ^{52}Mn due to the technique's improved separation factor [21].

The objective of this work is to develop the foundation for Mn-based PET and MRI and establish proof of concept regarding the potential of DMT1 as a dual-modality reporter gene for stem cell imaging in

the brain. With the complementary strengths of PET and MRI available, this approach may offer increased flexibility for *in vivo* cell tracking compared to other cell tracking approaches.

Methods

Target Construction and Irradiation

^{52}Mn was produced on a PETtrace cyclotron (General Electric Healthcare, Waukesha, WI, USA) by $^{nat}\text{Cr}(p,n)^{52}\text{Mn}$ using 16 MeV protons. Targets consisted of water jet cooled chromium discs (3/4" diameter, 0.4" thick, 99.95% pure, Kamis, Inc., Mahopac Falls, NY, USA). Target discs were machined to fit a cylindrical deplater for post irradiation etchings. Typical target masses obtained from etchings ranged from 70 to 400 mg over an area of 0.95 cm^2 . Depleted target masses were dependent upon the volume of acid used to etch the target face and the amount of time allowed for dissolution. Depleted masses were measured by weighing the dry target before and after etching. Co-production of the radioisotopic impurity ^{54}Mn ($t_{1/2} = 312.1$ d, $EC = 100\%$, $E_{\gamma} = 834$ keV) through $^{54}\text{Cr}(p,n)^{54}\text{Mn}$ was measured by high-purity germanium (HPGe) spectrometry (Canberra, Meriden, CT, USA). ^{52}Mn and ^{54}Mn production yields were compared to theoretical results calculated from experimental cross sections [22-24].

Separation Chemistry

The reported separation by Topping and colleagues uses a strong anion exchange resin and 12.1 M HCl as a mobile phase, with chromium eluting in early fractions and manganese eluting in later fractions [18]. This separation was conducted in our lab using 16 g of AG-1x8 (Bio-Rad, Hercules, CA, USA) in a glass column. The column was equilibrated with 70 ml Optima grade 12.1 M HCl (Sigma Aldrich, St. Louis, MO, USA). The irradiated and dissolved chromium target (70 ± 1 mg) contained in 7 mL of 11 M HCl was loaded onto the column, and 1-5 ml fractions were eluted using concentrated HCl. Eluted fractions were assayed for ^{52}Mn activity using a ionization well chamber (Capintec, Ramsey, NJ, USA), and chromium content was measured by microwave plasma atomic emission spectrometry (MP-AES; Agilent Technologies, Santa Clara, CA, USA). A Capintec dose calibrator setting (695/2) was obtained from cross-calibration with a well-characterized high purity germanium (HPGe) detector. Capintec activity readings were attributed entirely to ^{52}Mn , based on the assumption that ^{54}Mn contributes negligibly to chamber ionization.

A second separation method was employed using trioctylamine as an organic extractant. Chromium targets were etched by 5 ml concentrated HCl for 60

minutes at 90 °C following irradiation. Based on the change in target mass during dissolution, a calculated amount of 12.1 M HCl was added to the target solution to yield an HCl concentration of 9M. Mn^{2+} ions were extracted from the target solution to 10 ml of 0.8 M trioctylamine (Sigma-Aldrich) in cyclohexane, leaving the bulk chromium in the aqueous phase. After isolating the organic phase, 10 ml 0.005 M NH_4OH was used to back-extract the Mn^{2+} ions to aqueous phase [21]. This purification cycle was conducted a total of three times to sufficiently reduce chromium contamination. Trace chromium, manganese, iron, nickel, and zinc contamination was measured by MP-AES following the first purification cycle of this separation.

Thin layer chromatography (TLC) was performed on four different samples to examine the chemical form of ^{52}Mn in the TOA extracted product. Sample 1 consisted of the TOA extracted product dried down and taken up in water. Sample 2 consisted of ^{52}Mn separated by ion exchange chromatography in HCl as a standard for $^{52}MnCl_2$. Sample 3 was created by treating $^{52}MnCl_2$ (sample 2) with NaOH to produce $^{52}Mn(OH)_2$. Sample 4 was produced by treating $^{52}MnCl_2$ with H_2O_2 to produce $^{52}MnO_x$ ($x = 1, 2$). These four samples were tested against five different mobile phases: H_2O , 0.1 M HCl, 1:1 MeOH : 10% NH_4OAc , 0.05 M DTPA, and 0.25 M NH_4OH .

Cell Culture

A line of human neural progenitor cells (hNPC; G010) has previously been established from fetal cortical tissue and expanded as previously described [8, 25]. For these experiments, frozen cell aggregates (passage 18-25) were thawed, slowly re-suspended in Dulbecco's modified Eagle's medium (DMEM, Sigma-Aldrich) and 10% DNase, transferred to cell maintenance medium, and maintained for at least two weeks before experiments were performed. Cell maintenance medium consisted of DMEM and Ham's F12 (Sigma-Aldrich) at a ratio of 7:3, supplemented with 1% penicillin/streptomycin/amphotericin (Life Technologies, Carlsbad, CA, USA), 1% N2 (Life Technologies), 100 ng/ml epidermal growth factor (Millipore, Billerica, MA, USA), 20 ng/ml fibroblast growth factor 2 (WiCell, Madison, WI, USA), 10 ng/ml leukemia inhibitory factor (Millipore), and 5 ng/ml heparin (Sigma-Aldrich) [8]. Approximately one-half of the conditioned cell media was removed and replaced with fresh pre-warmed maintenance media every 3-4 days. The cells were passaged by chopping every 10-14 days using a McIlwain automated tissue chopper (Mickle Laboratory Engineering Co. Ltd., Surrey, UK).

Transfection

An expression vector encoding the DMT1 protein under the cytomegalovirus promoter (SLC11A2 HaloTag Fusion FlexiVector) was acquired from the Promega Kazusa cDNA clone library (Promega, Madison, WI, USA) and used for cell transfection. The expression vector was introduced into hNPC using the Basic Primary Neurons Nucleofection system (Lonza Group, Basel, Switzerland). Cells were dissociated in DMEM after a 15-minute TrypLE treatment (Life Technologies). For each nucleofection reaction, five million cells were resuspended in nucleofection solution containing 4 μ g of the DMT1 expression vector, pulsed in the nucleofector device, and returned to pre-warmed maintenance media. After transfection, some cells were plated on pre-coated cover slips for immunochemical analysis. Coverslips were treated with poly-ornathine and poly-L-laminin (both from Sigma-Aldrich) to promote cell adherence, and 30,000 cells were plated per cover slip. The remaining cells were returned to suspension culture in a 6-well plate coated with poly-2-hydroxyethyl methacrylate to reduce adherence.

Immunocytochemistry

Immunocytochemistry was used to examine expression of the human DMT1 protein in hNPC. Cover slips were fixed with 4% paraformaldehyde (PFA) and washed with phosphate-buffered saline (PBS) before incubation in blocking buffer (PBS, 5% normal donkey serum (NDS), 0.2% Triton X-100 (Sigma-Aldrich)) for 30 minutes. The anti-DMT1 primary antibody (mouse monoclonal; Sigma-Aldrich) was diluted 1:500 in blocking buffer. Cells were incubated in primary antibody for 1 hour at room temperature then washed with PBS. Secondary antibody (donkey anti-mouse IgG Alexa Fluor 488; Jackson ImmunoResearch Laboratories, West Grove, PA, USA) was diluted 1:1,000 in blocking buffer and then applied to cells for 30 minutes. After another PBS wash, coverslips were incubated in Hoescht 33258 nuclear stain (Sigma-Aldrich) for 3 minutes before mounting coverslips on glass slides with Fluoromount (Southern Biotech, Birmingham, AL, USA). Images were collected using a Nikon Eclipse fluorescence microscope, a Nikon Intensilight camera, and NIS Element D software (Nikon, Tokyo, Japan). ImageJ software was used for image processing and cell counting. For each expression time point, at least six fields of view on each of three coverslips were analyzed for percent of cells over-expressing DMT1.

Cell Viability Assay

To examine the potential acute toxicity of combined DMT1 expression and Mn supplementation on

hNPC, a trypan blue cell viability assay was performed. Cells were transfected to express DMT1, and a control group of cells were subject to the transfection procedure without introducing the DMT1 expression vector. Cells were then returned to floating culture in maintenance media. One day later, cell samples were supplemented with 0, 100, or 1000 μM MnCl_2 and incubated for 24 hours. After collection and dissociation in DMEM, a small amount of the cell suspension was diluted in an equal volume of trypan blue (Sigma-Aldrich). Viable and unviable cells in each sample were counted, where unviable cells were characterized by blue dye infiltration. For each Mn dose and cell type, three individual samples were treated and analyzed. An unpaired two-tailed Student's t-test was used to compare the fraction of unviable cells between cell types and Mn supplementation levels.

In vitro MRI

In preparation for MRI, transfected cells and wild-type controls (hNPC-DMT1 and hNPC-WT, respectively) were supplemented with 0-400 μM MnCl_2 for one hour. Cell samples were then collected, allowed to settle, and rinsed several times to remove extracellular Mn^{2+} . They were then transferred to 0.25 ml microcentrifuge tubes and spun down to form cell pellets. Samples were stabilized in 1.5 ml microcentrifuge tubes filled with 4% agar gel. MR imaging was performed on a 4.7 T preclinical MRI scanner (Agilent Technologies). To observe the T_1 shortening effects of Mn^{2+} , T_1 mapping was performed using a 3D variable flip angle spoiled gradient echo (VFA SPGR) sequence [26]. Pulse sequence parameters were: TR=8.4ms, TE=3.48ms, flip angles (in degrees) = 5, 10, 15, 20, 30, 45, with gradient and RF spoiling. T_1 times were approximated with nonlinear least squares fitting of the signal data as a function of flip angle, and R_1 maps were calculated ($R_1 = 1/T_1$). This procedure was subsequently repeated to confirm the results.

In vitro ^{52}Mn uptake

To observe ^{52}Mn uptake in hNPC, cells were supplemented with 0-0.8 μCi (0-2.3 $\mu\text{Ci}/\mu\text{L}$) of ^{52}Mn in DMEM for one hour. In each cell sample, approximately equal numbers of either hNPC-DMT1 or hNPC-WT were used. After one hour, cells were spun down at 1000 rpm (62 g) for 4 minutes, and the supernatant was removed and replaced. This spin-down and removal step was repeated 3 times. ^{52}Mn uptake was measured by automatic gamma counting on a PerkinElmer Wizard 2480 (Waltham, MA, USA). Counts were measured for 300 seconds with gating centered on the 744 keV gamma peak. During the gamma counting procedure, remaining cell samples were re-counted using trypan blue to verify viable cell

numbers and to correct results based on respective cell numbers per sample. The final activity uptake in each sample was corrected by a known ^{52}Mn calibration factor (units activity per count rate), by a no-activity control, and based on number of cells per sample. The uncertainty of the Poisson-distributed counting data was propagated through each of these correction calculations. To confirm results, this experiment was repeated in a separate trial.

Animals

All animal studies were performed in accordance with protocols approved by the University of Wisconsin Institutional Animal Care and Use Committee. Adult wild-type male and female Sprague-Dawley rats (age 80-240 days) were used for cell transplantation and imaging experiments. Rats were housed under controlled temperature and illumination conditions, with unrestricted access to food and water. Cyclosporine (10 mg/kg) was administered to rats intraperitoneally (i.p.) beginning one day prior to cell transplantation until sacrifice. At the end of imaging studies, rats were anesthetized with 5% isoflurane, administered 0.2 ml pentobarbital i.p., and transcardially perfused with chilled 0.9% NaCl followed by 4% PFA.

Cell transplantation

Two days following transfection, hNPC-DMT1 and hNPC-WT were separately collected and resuspended at a concentration of 150,000 cells/ μL in transplantation media. Transplantation media consisted of Leibovitz L15 medium (Life Technologies) and PBS at a ratio of 1:1 supplemented with 2% B27 (Life Technologies) and 0.6% glucose. For transplantation procedures, rats were anesthetized with isoflurane and secured in a stereotaxic frame. Cells were injected bilaterally in two striatal sites (AP +0.5 mm and -0.1 mm; ML ± 3.3 mm and ± 2.8 mm; DV -4.5 mm) with 2-3 μL cells (150,000 cells/ μL) per site. A 10 μL Hamilton Syringe with a 30-gauge sharp tip needle was secured to the stereotaxic frame before needle insertion and cell injection. For each injection site, the needle was slowly lowered into the striatum, maintained at that location for 2 minutes, cells were injected at a rate of 1 $\mu\text{L}/\text{min}$, and the needle was left for 2 additional minutes and then slowly removed [8, 27]. Transfected hNPC-DMT1 were transplanted in the right striatum, while hNPC-WT were transplanted in the left striatum.

In vivo MRI

Three animals have undergone MR imaging after cell transplantation. One day following surgeries, animals were injected with 50 mg/kg of MnCl_2 (dissolved in bicine buffer to a concentration of 100 mM).

Fourty-eight and 72 hours later, the animals were anesthetized with isoflurane and scanned with the same 3D VFA SPGR scan for T₁ mapping as was used for *in vitro* imaging. T₁ mapping was performed and R₁ maps were calculated as described above.

In vivo PET

Two animals have undergone PET/CT imaging after cell transplantation. One day following cell transplantation, animals were systemically injected with approximately 0.85 mCi ⁵²Mn. One of these subjects (subject 1) received no-carrier-added ⁵²Mn in saline, while the other (subject 2) received ⁵²Mn in 100mM MnCl₂ in bicine to mimic the contrast agent delivered for MR imaging. Twenty-four hours after contrast administration, animals were anesthetized with isoflurane and scanned on a Siemens Inveon microPET/CT (Siemens Medical Solutions, Erlangen, Germany). PET images were reconstructed as a single static segment using scatter-corrected OSEM reconstruction. The brain of subject 2 was resected for *ex vivo* brain PET/CT. Sections of 1 mm thickness were cut with a razor and a rat brain matrix slicer, and autoradiographs of these brain sections were collected.

Histology

After perfusion, brains were submerged in PFA for an additional 24 hours before being switched to 30% sucrose. Thirty-micron slices were sectioned with a frozen stage microtome. Immunohistochemistry was performed using primaries against human glial fibrillary acidic protein (GFAP) to detect transplanted neural progenitors (anti-hGFAP mouse monoclonal, StemCells, Inc., Cambridge, UK) and human DMT1 to observe DMT1 over-expression in transplanted cells (mouse monoclonal anti-hDMT1, Sigma-Aldrich). Brain sections were washed in PBS (3×5 minutes) then blocked in blocking buffer (PBS, 3% NDS, 0.25% Triton X-100) for 1 hour at room temperature (RT). Sections were then transferred to primary antibody diluted 1:200 in blocking buffer and incubated overnight at RT. PBS washes (3×5 minutes) were performed before secondary antibody incubation (donkey anti-mouse AF488 antibody 1:500 in blocking buffer) for one hour. Sections were mounted on glass slides with DAPI mounting medium and examined with a Nikon fluorescence microscope.

Results

Target Construction and Irradiation

Water jet cooled chromium targets withstood beam currents of 30 μA for two hours with no visible aberration. After four target irradiations and etchings, some pitting became noticeable on the target face. The chromium target withstood six etchings before the

deplater o-ring seal was compromised (**Figure 1B**). A HPGe spectrum was collected for radioisotopic purity measurements and is shown in **Figure 1A**. Isotope yield predictions and measurements are summarized in **Table 1**. Measured thick target ⁵²Mn production rate with 16 MeV protons was found to be 0.256 ± 0.022 mCi/μAh, 13% less than the yield predicted by experimental cross section data [22-24]. Measured ⁵⁴Mn production rates were in good agreement with predictions. Despite the relatively large ⁵⁴Mn cross section, production was expected to be minimal due to the low natural abundance of ⁵⁴Cr (2.4%). ⁵⁴Mn decays by electron capture emitting a 835 keV gamma. Such a decay would have a negligible effect on image quality, but would contribute to patient dose clinically. ⁵¹Cr is also produced by ⁵²Cr (p,pn)⁵¹Cr and by the decay of ⁵¹Mn produced through ⁵²Cr(p,2n)⁵¹Mn, but this contaminant was easily removed during target separation chemistry. An end of bombardment (EoB) radionuclidic purity of 99.55% was calculated from yield measurements, which was sufficiently high for our purposes.

Table 1: Experimental yields for the production of ⁵²Mn and ⁵⁴Mn with 16 MeV protons on a thick target as measured by HPGe spectrometry compare well to theoretical yields calculated from measured nuclear cross sections [22-24]. Experimental and theoretical radionuclidic purities agree well.

	Experimental	Theoretical
⁵² Mn Yield	0.256 ± 0.022 mCi/μAh	0.291 mCi/μAh
⁵⁴ Mn Yield	1.14 ± 0.14 μCi/μAh	1.161 μCi/μAh
⁵² Mn Purity	99.55%	99.60%

Separation Chemistry

The radiochemistry of Mn/Cr can be challenging due to the presence of multiple oxidation states of both elements and the similar chromatographic behavior of Mn(II) and Cr(III) [28]. The separation used by Topping and colleagues employs the AG-1x8 anion exchange resin and concentrated HCl as a mobile phase. Alternatively, trace Mn has been separated from chromium metal using the organic extractant trioctylamine (TOA), first reported by Lahiri *et al.* [21]. For *in vivo* applications, it is essential that trace Cr is minimized in the injected product due to its significant toxicity [29]. In our production of ⁵²Mn, both methods were used as a preliminary attempt to compare and assess efficacy, yield, and chemical purity.

Our radiochemical separation using AG-1x8 resulted in the elution profile shown in **Figure 1C**. Combining fractions from 40 mL to 86 mL resulted in 60.1% activity recovery with 0.872 mg ^{nat}Cr metal remaining in the product, as measured by MP-AES. This corresponds to a separation factor of approximately

68. Furthermore, late fractions containing only trace chromium still eluted as a yellow color, suggesting the AG-1x8 resin was being degraded by concentrated HCl.

In the solvent-solvent extraction separation, from a starting bulk chromium mass of 456 ± 1 mg, a post-separation chromium mass of 5.35 ± 0.04 ng was measured by MP-AES. This mass reduction corresponds to an average separation factor of 440.1 for each of the three purification cycles. Each cycle had a ^{52}Mn recovery efficiency of $73 \pm 7\%$ ($n=6$), resulting in an overall separation efficiency of approximately 35%. These efficiencies and separation factors agree reasonably well with the work conducted by Lahiri *et al* [21]. Trace metal analysis results by MP-AES (Cr, Mn, Fe, Ni, and Zn) for the TOA extracted ^{52}Mn product are summarized in Supplementary Material: **Table S1**. Following the three separations, the ^{52}Mn in 0.005 NH_4OH solution was passed through a C-18 Sep-Pak to remove any residual organic phase. The product was dried under argon overflow then reconstituted in PBS. All further *in vitro* and *in vivo* work with ^{52}Mn was conducted using this TOA extraction technique, as it was capable of reducing chromium impurities to trace levels with acceptably high ^{52}Mn recovery.

To confirm that the TOA separated ^{52}Mn product was indeed in the MnCl_2 or Mn^{2+} chemical form, thin layer chromatography (TLC) experiments were performed to rule out $\text{Mn}(\text{OH})_2$ and MnO_x as possible insoluble species. Thin layer chromatography was performed using four different samples: (1) TOA extracted product in water, (2) ion exchange chroma-

tography product in HCl as a $^{52}\text{MnCl}_2$ standard, (3) $^{52}\text{Mn}(\text{OH})_2$, and (4) $^{52}\text{MnO}_x$. In the five mobile phases tested, samples 1 and 2 acted nearly identically, implying that the TOA product was not in the insoluble forms $\text{Mn}(\text{OH})_2$ or MnO_x (**Figure 2**). From these TLC results, we concluded that the TOA separated ^{52}Mn product was likely in the MnCl_2 or Mn^{2+} state.

DMT1 over-expression

In order to use Mn-based contrast agents for cell tracking applications, we first induced over-expression of DMT1 in hNPC to increase the uptake of Mn^{2+} in these cells. The Lonza Nucleofection system was used for this purpose. This is a relatively simple method to induce transient protein expression, which we have previously used for proof-of-concept investigations of cell tracking methods [8]. To identify altered protein expression, transfected and wild-type cells (hNPC-DMT1 and hNPC-WT) were plated immediately after transfection, fixed over the course of 10 days after plating, and stained with an antibody against human DMT1. Sufficient reporter gene expression was detected in the transfected cell population, with up to 42% of cells over-expressing DMT1 one day following transfection (**Figure 3A**). Over the course of 10 days after plating, the percentage of cells over-expressing DMT1 decreased steadily (**Figure 3B**). All further experiments were carried out using unsorted hNPC-DMT1 as soon after nucleofection as possible to maximize the portion of hNPC over-expressing the reporter.

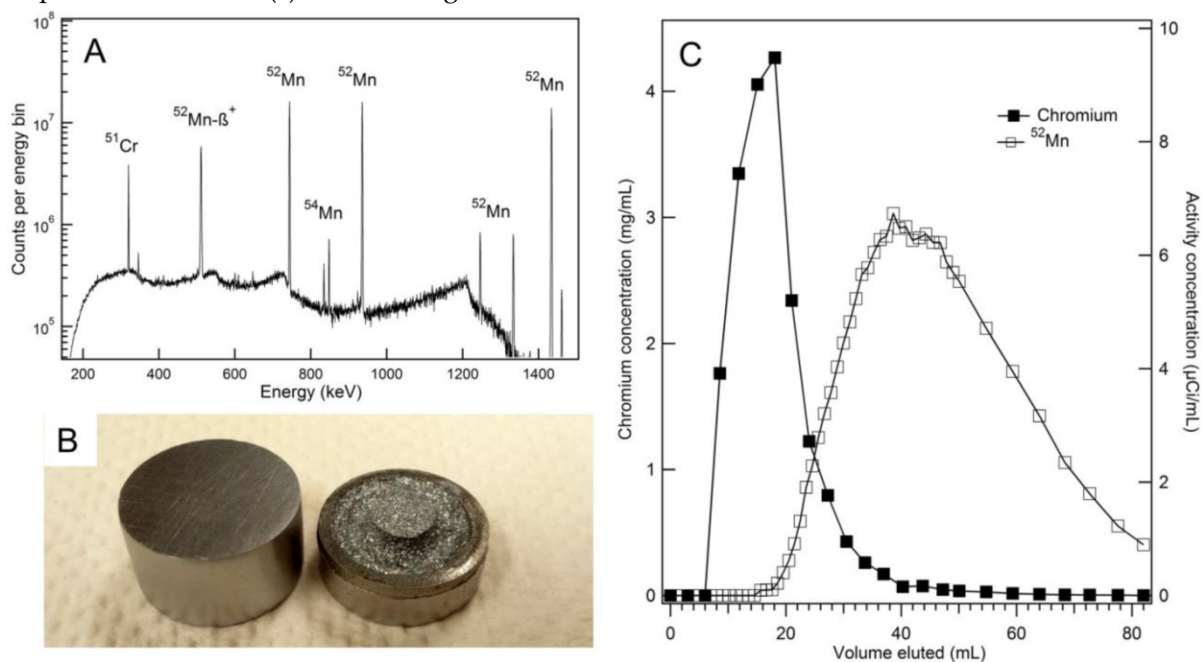


Figure 1: (A) An efficiency corrected high-purity germanium (HPGe) spectrum of unseparated target material collected nine days post-irradiation shows minimal ^{54}Mn contamination. (B) New chromium discs (left) are machined to produce a target which fits tightly into deplater. After six etchings, significant pitting on the target face and a loss of o-ring integrity was observed (right). (C) The elution profiles for bulk chromium and ^{52}Mn on an AG-1x8 column using concentrated HCl show some overlap. Chromium concentrations were measured by microwave plasma atomic emission spectrometry (MP-AES), and activity concentrations were measured by an ionization well chamber.

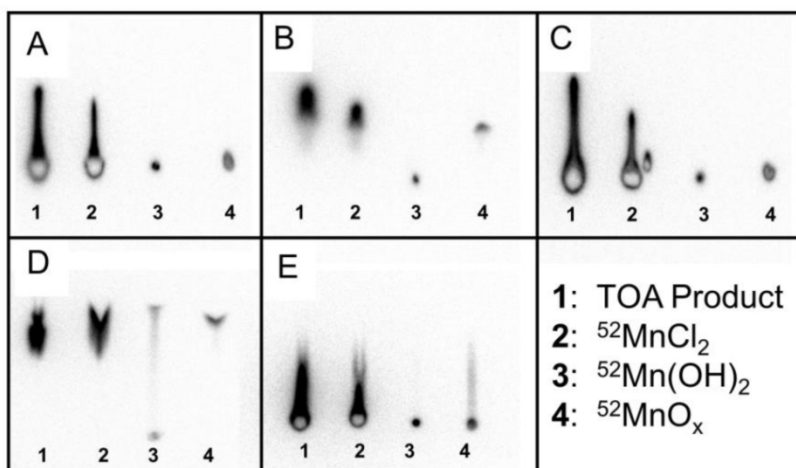


Figure 2: Mn(OH)_2 and MnO_x ($x = 1, 2$) were assumed to be the most likely insoluble and non-dissociative alternative chemical forms to MnCl_2 following separation by TOA extraction. Standards were prepared and tested against five different mobile phases using thin layer chromatography (TLC). The five mobile phases were (A) H_2O , (B) 0.1 M HCl, (C) 1:1 MeOH:10% NH_4Ac , (D) 0.05 M DTPA, (E) 0.25 M NH_4OH . In these TLC activity distributions, the TOA product and $^{52}\text{MnCl}_2$ standard behave the same way for all five mobile phases. The TOA product and $^{52}\text{MnCl}_2$ standard do not behave exactly like the $^{52}\text{Mn(OH)}_2$ and $^{52}\text{MnO}_x$ standards for any mobile phase. These results imply that our TOA product is in the Mn^{2+} form after being taken up from dryness in water.

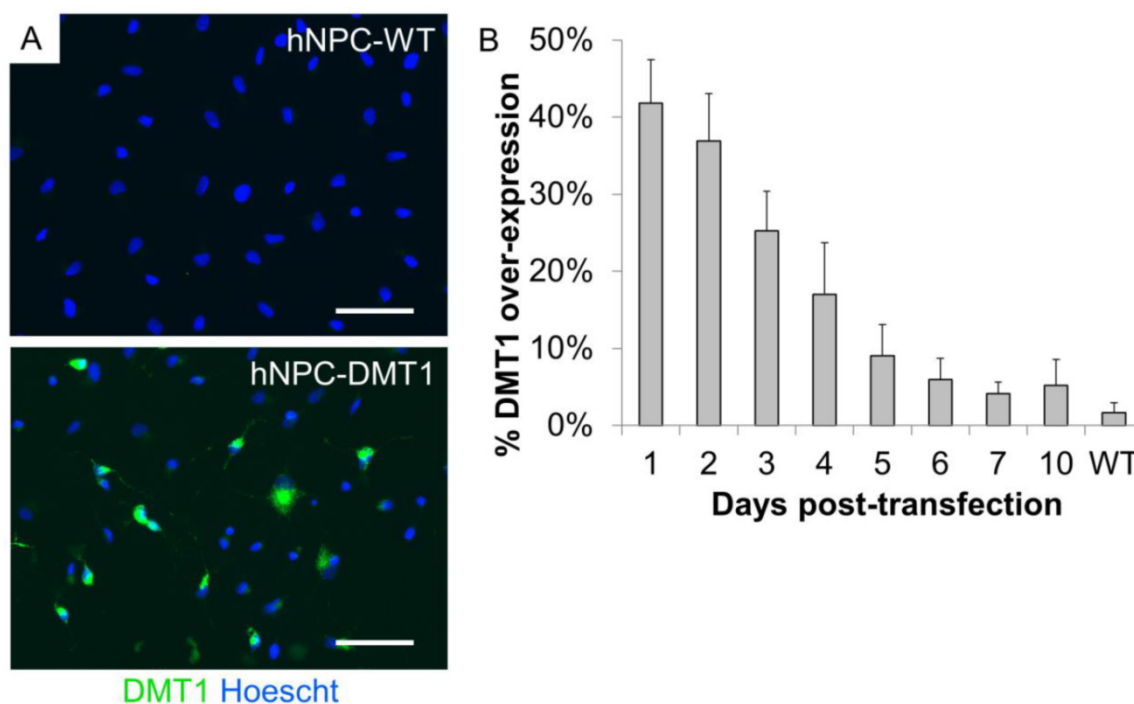


Figure 3: (A) Immunocytochemistry of hNPC one day following transfection shows that transfected cells express high levels of the DMT1 protein when compared to wild-type cells. (B) After plating transfected and wild-type cells and fixing each day for 10 days, counts of DMT1 over-expressing cells reveal that DMT1 expression decreases toward background (wild-type) levels over the course of 10 days. Scale bar = 50 μm .

Cell viability assay

The potential toxic effects of manganese on both organisms and neural progenitor cells must be understood before application of this imaging technique in preclinical cell therapy experiments [30, 31]. An *in vitro* toxicity assay was performed to observe whether DMT1-expressing cells exhibit increased sensitivity and cell death in response to manganese exposure. Cells were supplemented with MnCl_2 at concentra-

tions of 0, 100, or 1000 μM for 24 hours. The concentration of 100 μM was selected to reflect the approximate expected Mn^{2+} concentration in the rat brain after a systemic injection of MnCl_2 at typical doses used for MEMRI [32], whereas the concentration of 1000 μM was used as a positive control. The results of the trypan blue cell viability assay are shown in **Figure 4**. Approximately 20% of cells were found to be unviable even in samples not supplemented with manganese due to the detrimental effects of the nu-

cleofection solution and transfection procedure on hNPC. For this reason, hNPC-WT subjected to the nucleofection procedure without the introduction of the DMT1 expression plasmid were used as a control in this study. After 100 μM MnCl_2 supplementation, neither hNPC-DMT1 nor hNPC-WT showed significantly decreased cell viability, and they did not differ significantly from one another. However, at a manganese concentration of 1000 μM , these differences became significant. This concentration is far greater than that required for imaging experiments, either *in vitro* or *in vivo*. This study confirmed that this imaging approach is not a significant cause of acute cell toxicity in this application and prompted further *in vitro* and *in vivo* imaging experiments.

In vitro MRI

To investigate whether DMT1 over-expressing cells internalize sufficient Mn^{2+} for T_1 -weighted MRI

contrast, Mn^{2+} uptake was compared in hNPC-DMT1 and hNPC-WT. Cells were supplemented with 0-400 μM MnCl_2 for one hour. The cells were rinsed, spun down into pellets, and imaged with a 3D VFA SPGR sequence for T_1 mapping. The R_1 relaxation rate, which is the inverse of T_1 relaxation time, was calculated from T_1 maps. The resulting R_1 maps of hNPC-WT and hNPC-DMT1 are shown in **Figure 5**. At all MnCl_2 concentrations, clear contrast was observed between hNPC-DMT1 and hNPC-WT. Importantly, this difference was easily discernable at biologically relevant concentrations of 50-100 μM . A slight increase in R_1 of hNPC-DMT1 is observed even without MnCl_2 (0 μM). This may be due to low levels of iron in the cell maintenance media, which is transported by DMT1 and is a weak T_1 -shortening agent.

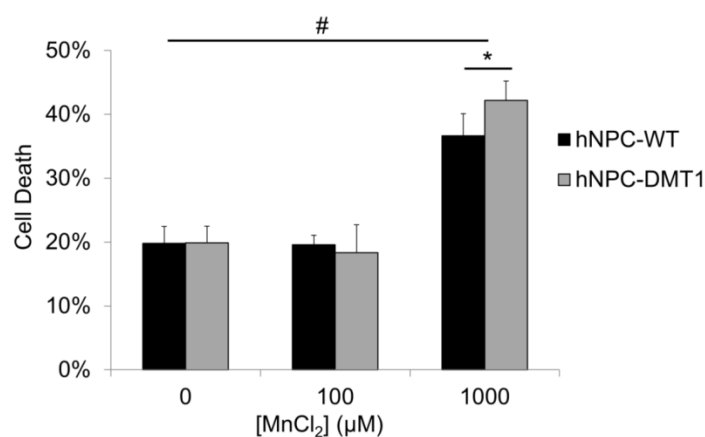


Figure 4: Trypan blue cell exclusion assay results reveal no significant increase in hNPC death after 24 hour exposure to 100 μM MnCl_2 , a concentration on the order of that expected in the brain after systemic MnCl_2 delivery. At this concentration, consistent results are observed for hNPC-WT and hNPC-DMT1. Cell death is observed at 0 μM due to the potentially toxic effects of the transfection solution and procedure on cells. The positive control dose of 1000 μM resulted in a significant increase in cell death for both cell types as well as a significant increase of hNPC-DMT1 death compared to hNPC-WT. #: $p < 0.05$ compared to corresponding cell type supplemented with 0 μM MnCl_2 ; *: $p < 0.05$ compared to hNPC-WT supplemented with same dose.

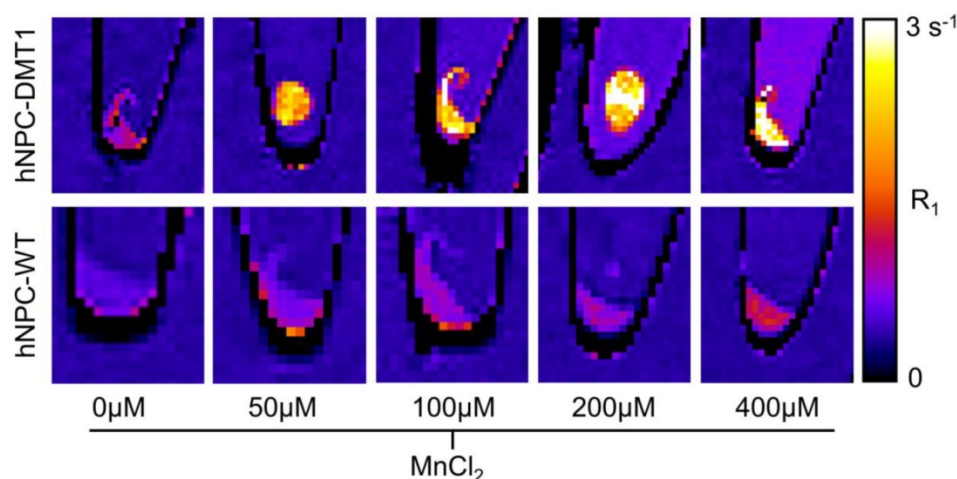


Figure 5: Representative R_1 relaxation rate maps of hNPC-DMT1 (top row) and hNPC-WT (bottom row) after 1-hour supplementation with MnCl_2 at a range of concentrations. Clear contrast is observed between hNPC-WT and hNPC-DMT1 at all MnCl_2 concentrations tested.

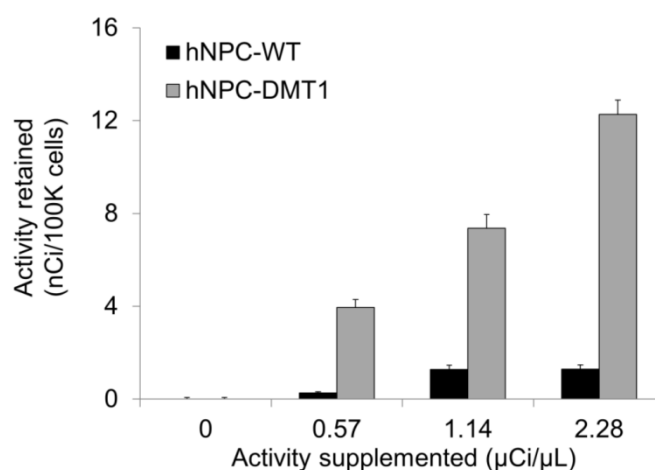


Figure 6: hNPC-DMT1 show increased ^{52}Mn uptake compared to hNPC-WT after a one-hour incubation as measured by gamma counting (representative results from one trial shown). Error bars represent propagated error from Poisson-distributed counting data.

Gamma counting of ^{52}Mn uptake *in vitro*

Using the ^{52}Mn produced in our lab, we could both directly measure Mn uptake in hNPC-DMT1 and further assess whether enhanced uptake compared to hNPC-WT was achieved. The cell preparation procedure outlined above for *in vitro* MRI was mirrored for gamma counting of cellular ^{52}Mn uptake. After a 1-hour incubation with 0-0.8 µCi of no-carrier-added ^{52}Mn , cells were spun down and rinsed to remove extracellular manganese. Gamma counting was used to compare the relative uptake of ^{52}Mn in hNPC-DMT1 and hNPC-WT. Manganese uptake increased linearly with supplemented activity for both cell types, and hNPC-DMT1 showed strikingly increased retained activity when compared with hNPC-WT (Figure 6). In a parallel study, cells were supplemented with 0-0.8 µCi of ^{52}Mn in 50 µM MnCl_2 , and identical gamma counting results were obtained (data not shown). These results demonstrate that DMT1 over-expressing cells show increased uptake of manganese-based contrast agents, even at tracer levels of supplemented ^{52}Mn . These *in vitro* results prompted studies of cell detectability with *in vivo* MRI and PET.

In vivo MR imaging

For proof of concept *in vivo* cell detection with MRI, three rats were transplanted with hNPC-DMT1 in the right striatum and hNPC-WT in the left. Two days later, MnCl_2 was delivered systemically in preparation for MR imaging. At 48 and 72 hours later, the animals were imaged with a T_1 mapping sequence to observe the T_1 shortening effects of Mn^{2+} . After imaging and perfusion, histological evaluation was performed to verify cell survival through the transplantation and imaging procedure. In two of the three MRI subjects, a region of increased R_1 was observed in

the right striatum (Figure 7). This contrast corresponds to the location of transplanted hNPC-DMT1, detected histologically with antibodies against human GFAP (used to detect human cells) and human DMT1 (Figure 8). Wild-type cells transplanted contralaterally were also detected histologically, ruling out the possibility that hNPC-WT were undetectable in MRI simply due to cell death. These preliminary *in vivo* results, along with the Mn^{2+} uptake measured *in vitro*, strongly support our hypothesis that high levels of manganese are taken up in DMT1 over-expressing hNPC, permitting *in vivo* visualization with MRI.

However, in one of the three subjects, a decrease in R_1 was observed in the vicinity of hNPC-DMT1 (Figure 7C). In this same region, T_2 -weighted imaging showed a hypointense region corresponding to cell location (Supplementary Material: Figure S1A). This is likely due to surgery-induced hemorrhage in the brain, which we have found to be a challenging confounding factor in MRI of transplanted hNPC. Iron accumulation was detected with Prussian blue staining and could wipe out MR signal, making T_1 calculation impossible (Supplementary Material: Figure S1B).

In vivo and ex vivo PET imaging

For initial observation of ^{52}Mn uptake in the brain and in transplanted hNPC, PET/CT (combined PET and computed tomography) imaging was performed in two rats. Rats were systemically delivered 0.85mCi ^{52}Mn two days after cell transplantation and imaged 24 hours later. One rat received ^{52}Mn in saline, while another received ^{52}Mn supplemented with 100µM MnCl_2 in bicine to mimic the MRI contrast administration and bulk manganese dynamics. ^{52}Mn was taken up in the gastrointestinal system, bone, and areas of inflammation, but low brain uptake was detected *in vivo* in both subjects (Figure 9A). *Ex vivo*

PET/CT showed low levels of brain uptake, with slightly increased ^{52}Mn levels in the right striatum, corresponding to the location of hNPC-DMT1 (Figure 9B). Autoradiographs also indicated low but detectable levels of ^{52}Mn in the brain, with increased activity

in the vicinity of transplanted hNPC-DMT1 (Figure 9C). These initial results indicate that although ^{52}Mn -based PET imaging in the brain does not directly mirror MEMRI results, DMT1 shows potential for ^{52}Mn PET-based cell detection in the brain.

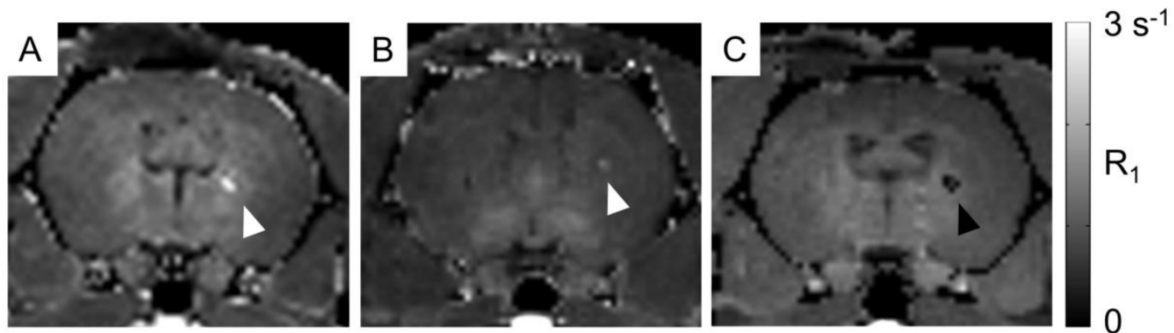


Figure 7: *In vivo* manganese-enhanced MRI of rats after hNPC-DMT1 transplantation. (A and B) In two of three subjects, hNPC-DMT1 were detectable on R_1 maps (white arrowheads). (C) In one subject, T_1 mapping failed in the vicinity of hNPC-DMT1, possibly due to hemorrhage-related iron accumulation (black arrowhead).

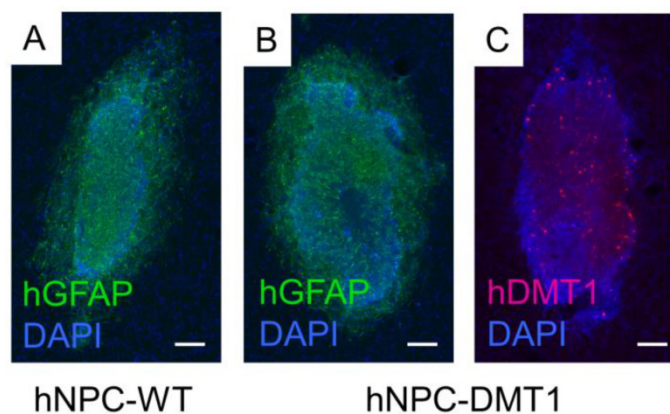


Figure 8: Immunofluorescence against human GFAP confirmed that both hNPC-WT (A) and hNPC-DMT1 (B) survived after transplantation and imaging. (C) Transfected cells continued to over-express the human DMT1 protein after transplantation. hNPC-WT staining for hDMT1 is negative (data not shown). Scale bar = 100 μm .

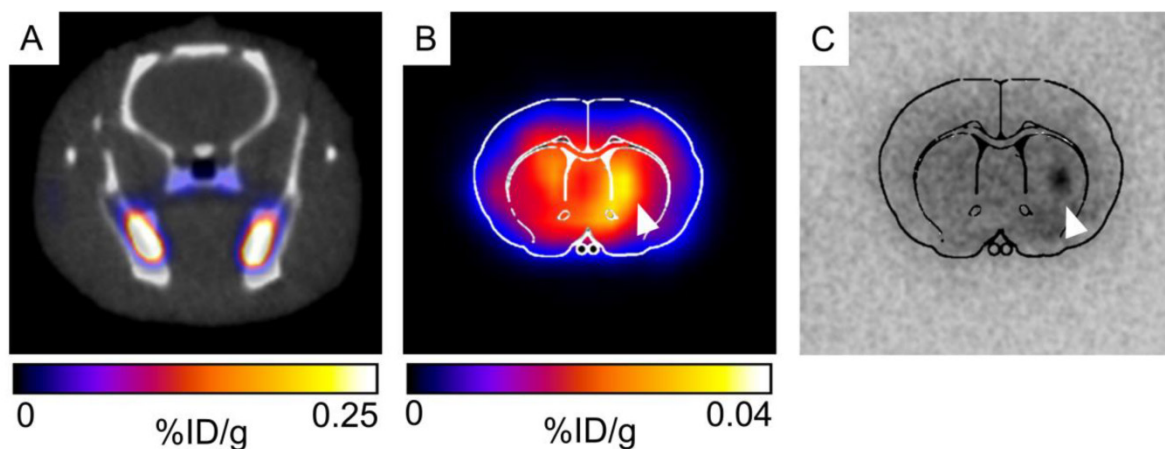


Figure 9: (A) Very low brain uptake is observed in ^{52}Mn -based PET/CT imaging *in vivo*. (B) When the brain is excised and imaged *ex vivo*, low levels of brain uptake are detectable. Both *ex vivo* imaging and autoradiography indicated that increased levels of ^{52}Mn are retained in the vicinity of hNPC-DMT1 (white arrowhead, B and C).

Discussion

In this work, we have performed ^{52}Mn production and separation experiments along with *in vitro* and *in vivo* imaging studies to lay the foundation for a new dual-modality approach for stem cell imaging in the central nervous system. To make high-purity ^{52}Mn for *in vivo* applications, two ^{52}Mn separation techniques based on ion exchange chromatography and solvent-solvent extraction were performed and evaluated. The solvent-solvent extraction technique was preferred due to improved ^{52}Mn recovery and reduced Cr impurities. To investigate the potential of DMT1 as a reporter gene for *in vivo* stem cell tracking with manganese-based PET and MRI, we induced over-expression of DMT1 in hNPC. *In vitro* supplementation of $^{52}\text{MnCl}_2$ and $^{nat}\text{MnCl}_2$ was used to compare manganese uptake in hNPC-DMT1 and hNPC-WT with gamma counting and T1 relaxation measurements, and we observed enhanced Mn uptake in hNPC-DMT1. Finally, in proof-of-concept studies for *in vivo* cell tracking, hNPC-DMT1 were transplanted into the striatum of adult wild-type rats. Contrast due to increased Mn uptake in transplanted hNPC-DMT1 was detected with *in vivo* MEMRI and *in vivo* PET and autoradiography.

For the thick target production of ^{52}Mn using unenriched chromium, a radioisotopic purity of 99.55% was obtained in this work. Cross section data suggest that ^{54}Mn production could be further reduced by irradiating a thin target ($\sim 70\ \mu\text{m}$) at 16 MeV rather than the thick target technique [22-24]. Theoretical calculations show that this technique could improve ^{52}Mn purity to 99.9%, a 4x reduction in ^{54}Mn . The disadvantages of such a thin target approach would be a drastic reduction in production capacity and an increase in target expense. The major elemental impurity found in our TOA separated ^{52}Mn product as measured by MP-AES was natural manganese metal (8.13 μg in one separated ^{52}Mn batch), which suggests that Mn is a significant impurity in the 99.95% elementally pure Cr target discs. Although our present work has no specific activity requirement, it is possible that future applications will require a more pure chromium target. A manganese-free chromium target could possibly be obtained by the electrodeposition of previously separated chromium metal on an inert backing material, much like the targetry technique commonly used for ^{64}Cu production [33]. However, for dual-modality applications, natural manganese in the ^{52}Mn product is of little concern as higher levels of natural manganese are necessary for MRI contrast.

The radiochemical separation of ^{52}Mn from chromium metal using anion exchange chromatog-

raphy yielded a lower than expected separation factor of 68 with 60.1% ^{52}Mn recovery. Our work shows a significant discrepancy in the quantity of resultant chromium metal when compared to the results by Topping *et al.* [18]. This discrepancy is perhaps due to column volume, initial target mass, or the solution volume used to load the target material. Future attempts to utilize this separation technique will employ a slightly larger column volume, as well as a more concentrated target solution ($< 2\text{mL}$). Furthermore, before this separation is used to produce an injectable ^{52}Mn product, the yellow eluent color must be characterized as it possibly indicative of resin degradation.

Radiochemical separation by iterative TOA extraction was found to be highly effective (440 separation factor; ^{52}Mn recovery = $73 \pm 7\%$, per cycle), but was more time consuming than ion-exchange chromatography due to the multiple dry-down steps. In the future, a trap and release type separation using a TOA functionalized resin could offer fast separation, small elution volumes, and a high separation factor. In all, our production and separation technique resulted in a product of sufficient quality for application of ^{52}Mn in the study of DMT1 as a dual-modality reporter gene for stem cell tracking.

In vitro assays were used to confirm DMT1 expression by transfected cells and to test the potential toxicity of combined DMT1 expression and manganese supplementation. The observation of slowly decreasing DMT1 over-expression is acceptable for these proof-of-concept studies and has been previously observed in our other reporter gene studies [8]. However, a line of cells stably expressing DMT1 needs to be developed for long-term cell tracking, detecting cell graft rejection, and more thoroughly characterizing the effect of this imaging technique on hNPC dynamics. The cell viability study showed that transient DMT1 over-expression and Mn supplementation did not have significant effects on cell viability at relevant concentrations for *in vivo* MRI, in agreement with previous studies investigating combined DMT1 expression and Mn supplementation on cells [15]. However, investigations of the effects of Mn on hNPC show more significant toxicity and indicate that trypan blue may not be the most sensitive method for detecting effects on cell viability [31]. The cell viability study further showed that extremely high concentrations of Mn have significant detrimental effects on cells. This result indicates the value of minimizing the supplemented Mn concentration, which a ^{52}Mn PET tracer may help accomplish. The toxicity at high concentrations also indicates that combined DMT1 expression and Mn supplementation does indeed harm cells and prompts future studies into the variety of

mechanisms by which viability is affected. For this purpose, a line of stably expressing hNPC-DMT1 will allow more flexibility and longevity in studies of toxicity and cell dynamics. Future studies with stable DMT1 over-expressing cells will more thoroughly investigate the effects of DMT1 expression and manganese supplementation on cell differentiation, proliferation, and viability over a longer period of time. However, for the purposes of this proof of concept work, the lack of significant toxicity at imaging-relevant concentrations encouraged the initiation of imaging studies.

Both *in vitro* MRI and ^{52}Mn gamma-counting experiments confirmed our hypothesis that hNPC-DMT1 take up higher levels of manganese than their wild-type counterparts. These studies indicated that this technique may be sufficiently sensitive for *in vivo* applications, and were in agreement with a previous study of DMT1 as an MEMRI reporter gene [15]. Indeed, *in vivo* MEMRI of hNPC-DMT1 confirmed that in the absence of confounding signal dropout, manganese uptake was sufficient to increase the R_1 relaxation rate. This permitted visualization of hNPC-DMT1, but not hNPC-WT, on R_1 maps. Histological confirmation of survival of both cell types confirmed that T_1 contrast specific to DMT1-expressing cells is observed. However, one subject did not show R_1 increase, likely because of iron deposition as a result of the surgery procedure. Iron is a potent T_2^* -shortening contrast agent and can cause regions of signal dropout, as observed in Supplementary Material: **Figure S1A**. It is also possible that the manganese concentration was high enough to significantly reduce T_2 relaxation time, muting signal from the region of high Mn^{2+} uptake. Other researchers have observed similar effects when mononuclear cells were pre-labeled with Mn before transplantation and MRI [16].

On the other hand, *in vivo* ^{52}Mn PET studies revealed very low brain Mn uptake. This was a surprising result, because brain uptake of Mn over the course of 24 hours has been observed in a variety of MEMRI studies [32]. Upon further investigation with *ex vivo* PET and autoradiography, low levels of activity in the brain were detected, with higher activity in the vicinity of hNPC-DMT1. Though encouraging, these results prompt further investigations into the biodistribution and temporal dynamics of ^{52}Mn after systemic delivery, which will be essential to establish the applicability of this imaging technique in the brain. These results also indicate that careful examination of the cellular and brain uptake of natural Mn and ^{52}Mn both in the presence and absence of one another is essential.

The results of this work indicate several avenues

of future investigation. Most importantly, a stable DMT1-expressing cell line will open doors for a variety of future studies. These studies will probe the long-term potential of this cell tracking technique, the ability to detect cell death or differentiation, and the long-term effects of DMT1 expression and manganese supplementation on cell dynamics. Furthermore, this approach could also be explored for direct labeling of cells. Cells transiently or stably over-expressing DMT1 could be incubated with Mn-based contrast agents prior to cell transplantation. PET and MRI could then be performed for an estimated 2-3 weeks after surgery to detect cell location and graft integrity. Although this approach would suffer the same weaknesses as other direct labeling methods, it could be used for dual-modality cell detection and would eliminate the need for systemic manganese delivery.

In conclusion, in this work we have established proof-of-concept for a novel dual-modality imaging approach. First, ^{52}Mn was produced by 16 MeV proton irradiation of chromium metal, followed by radiochemical isolation using two distinct separation techniques. The results of these studies indicate that ^{52}Mn production and separation for PET imaging is feasible. Then, $^{52}\text{Mn}^{2+}$ PET and MEMRI were used to establish the potential of DMT1 as a reporter gene for neural stem cell tracking in the rat brain. Importantly, this dual-modality manganese-based PET/MRI approach may have broad applications beyond cell tracking in the brain, including neuronal tract tracing, brain activation-induced uptake measurement, and cell tracking in other anatomy. Furthermore, we have confirmed that DMT1 is a compelling reporter gene candidate for stem cell detection with both MRI and PET. This work prompts further investigations into the potential of DMT1 for providing functional information regarding cell fates, including long-term survival, migration, and differentiation.

Supplementary Material

Figure S1 and Table S1.

<http://www.thno.org/v05p0227s1.pdf>

Acknowledgements

The authors gratefully acknowledge Promega Corporation for supplying the DMT1-HaloTag Fusion FlexiVector and Samuel A. Hurley, Ph.D., for his input regarding the acquisition and processing of T_1 mapping data. We thank our funding sources, including the US Department of Energy (DE-SC0008384), the National Institutes of Health (T32 GM008349 to C.M.L., NIBIB/NCI 1R01CA169365 to W.C.), the National Science Foundation (DGE-1256259 to R.H.), and the ALS Association (J10IZ9 and 15-IIP-201 to M.S).

Competing Interests

The authors have declared that no competing interest exists.

References

- Makkar RR, Smith RR, Cheng K, et al. Intracoronary cardiosphere-derived cells for heart regeneration after myocardial infarction (CADUCEUS): a prospective, randomised phase 1 trial. *Lancet*. 2012; 379: 895-904.
- Feldman EL, Boulis NM, Hur J, et al. Intraspinal neural stem cell transplantation in amyotrophic lateral sclerosis: phase 1 trial outcomes. *Ann Neurol*. 2014; 75: 363-373.
- Li L, Jiang W, Luo K, et al. Superparamagnetic iron oxide nanoparticles as MRI contrast agents for non-invasive stem cell labeling and tracking. *Theranostics*. 2013; 3: 595-615.
- Janowski M, Walczak P, Kropiwnicki T, et al. Long-term MRI cell tracking after intraventricular delivery in a patient with global cerebral ischemia and prospects for magnetic navigation of stem cells within the CSF. *PLoS One*. 2014; 9: e97631.
- Lang C, Lehner S, Todica A, et al. Positron emission tomography based in-vivo imaging of early phase stem cell retention after intramyocardial delivery in the mouse model. *Eur J Nucl Med Mol Imaging*. 2013; 40: 1730-1738.
- Arbab AS, Thiffault C, Navia B, et al. Tracking of In-111-labeled human umbilical tissue-derived cells (hUTC) in a rat model of cerebral ischemia using SPECT imaging. *BMC Med Imaging*. 2012; 12: 33.
- Cianciaruso C, Pagani A, Martelli C, et al. Cellular magnetic resonance with iron oxide nanoparticles: long-term persistence of SPIO signal in the CNS after transplanted cell death. *Nanomedicine (Lond)*. 2014; 9: 1457-1474.
- Bernau K, Lewis CM, Petelinsek AM, et al. In vivo tracking of human neural progenitor cells in the rat brain using bioluminescence imaging. *J Neurosci Methods*. 2014; 228: 67-78.
- Ahn BC, Parashurama N, Patel M, et al. Noninvasive reporter gene imaging of human Oct4 (pluripotency) dynamics during the differentiation of embryonic stem cells in living subjects. *Mol Imaging Biol*. 2014; [Epub ahead of print].
- Koehne G, Doubrovin M, Doubrovina E, et al. Serial in vivo imaging of the targeted migration of human HSV-TK-transduced antigen-specific lymphocytes. *Nat Biotechnol*. 2003; 21: 405-413.
- Vande Velde G, Raman Rangarajan J, Vreys R, et al. Quantitative evaluation of MRI-based tracking of ferritin-labeled endogenous neural stem cell progeny in rodent brain. *Neuroimage*. 2012; 62: 367-380.
- Rodriguez-Porcel M, Wu JC, Gambhir SS. Molecular imaging of stem cells. In: Girard L, ed. *StemBook*. Cambridge, MA, Harvard Stem Cell Institute; 2008.
- Illing AC, Shawk A, Cunningham CL, et al. Substrate profile and metal-ion selectivity of human divalent metal-ion transporter-1. *J Biol Chem*. 2012; 287: 30485-30496.
- Au C, Benedetto A, Aschner M. Manganese transport in eukaryotes: the role of DMT1. *Neurotoxicology*. 2008; 29: 569-576.
- Bartelle BB, Szulc KU, Suero-Abreu GA, et al. Divalent metal transporter, DMT1: A novel MRI reporter protein. *Magn Reson Med*. 2012; [Epub ahead of print].
- Odaka K, Aoki I, Moriya J, et al. In vivo tracking of transplanted mononuclear cells using manganese-enhanced magnetic resonance imaging (MEMRI). *PLoS One*. 2011; 6: e25487.
- Daube ME, Nickles RJ. Development of myocardial perfusion tracers for positron emission tomography. *Int J Nucl Med Biol*. 1985; 12: 303-314.
- Topping GJ, Schaffer P, Hoehr C, et al. Manganese-52 positron emission tomography tracer characterization and initial results in phantoms and in vivo. *Med Phys*. 2013; 40: 042502.
- Lin YJ, Koretsky AP. Manganese ion enhances T1-weighted MRI during brain activation: an approach to direct imaging of brain function. *Magn Reson Med*. 1997; 38: 378-388.
- Pautler RG, Silva AC, Koretsky AP. In vivo neuronal tract tracing using manganese-enhanced magnetic resonance imaging. *Magn Reson Med*. 1998; 40: 740-748.
- Lahiri S, Nayak D, Korschinek G. Separation of no-carrier-added ⁵²Mn from bulk chromium: a simulation study for accelerator mass spectrometry measurement of ⁵³Mn. *Anal Chem*. 2006; 78: 7517-7521.
- Kailas SG, et al. Total (p,n) reaction cross-section measurements on Ti-50, Cr-54, and Co-59. *Phys Rev*. 1975; C12: 1789-1796.
- Levkovskij VN. Activation cross section nuclides of average masses (A=40-100) by protons and alpha-particles with average energies (E=10-50MeV). Moscow: Inter-Vesi. 1991.
- Wing JH, et al. (p, n) Cross Sections of V51, Cr52, Cu63, Cu65, Ag107, Ag109, Cd111, Cd114, and La139 from 5 to 10.5 MeV. *Phys Rev*. 1962; X01: 280-290.
- Svendsen CN, ter Borg MG, Armstrong RJ, et al. A new method for the rapid and long term growth of human neural precursor cells. *J Neurosci Methods*. 1998; 85: 141-152.
- Deoni SC, Rutt BK, Peters TM. Rapid combined T1 and T2 mapping using gradient recalled acquisition in the steady state. *Magn Reson Med*. 2003; 49: 515-526.
- Behrstock S, Ebert AD, Klein S, et al. Lesion-induced increase in survival and migration of human neural progenitor cells releasing GDNF. *Cell Transplant*. 2008; 17: 753-762.
- Schuman RP. Radiochemistry of manganese. In: *Radiochemistry CoNCSO*, ed. U. S. Atomic Energy Commission; 1971.
- Dayan AD, Paine AJ. Mechanisms of chromium toxicity, carcinogenicity and allergenicity: review of the literature from 1985 to 2000. *Hum Exp Toxicol*. 2001; 20: 439-451.
- Rivera-Mancia S, Rios C, Montes S. Manganese accumulation in the CNS and associated pathologies. *Biometals*. 2011; 24: 811-825.
- Tamm C, Sabri F, Ceccatelli S. Mitochondrial-mediated apoptosis in neural stem cells exposed to manganese. *Toxicol Sci*. 2008; 101: 310-320.
- Chuang KH, Koretsky AP, Sotak CH. Temporal changes in the T1 and T2 relaxation rates (DeltaR1 and DeltaR2) in the rat brain are consistent with the tissue-clearance rates of elemental manganese. *Magn Reson Med*. 2009; 61: 1528-1532.
- McCarthy DW, Shefer RE, Klinkowstein RE, et al. Efficient production of high specific activity ⁶⁴Cu using a biomedical cyclotron. *Nucl Med Biol*. 1997; 24: 35-43.